Available online at www.sciencedirect.com
ScienceDirect
Talanta 75 (2008) 740–747
Talanta
www.elsevier.com/locate/talanta

Labeled magnetic nanoparticles assembly on polypyrrole film for biosensor applications

H. Ben Fredj [a], S. Helali [a], C. Esseghaier [a], L. Vonna [b,*], L. Vidal [b], A. Abdelghani [a]

[a] *Unité de Recherche de Physique des Semi-conducteurs et Capteurs, IPEST, La Marsa 2070, Tunis, Tunisia*
[b] *Institut de Chimie des Surfaces et Interfaces CNRS-UPR9069, 15 Rue Jean Starcky, 68057 Mulhouse Cedex, France*

Received 20 July 2007; received in revised form 1 December 2007; accepted 7 December 2007
Available online 3 January 2008

Abstract

In recent years, conducting polymers combined with metallic nanoparticles have been paid more attention due to their potential applications in microelectronics, microsystems, optical sensors and photoelectronic chemistry. The work presented in this paper describes the preparation and characterization of a nanocomposite composed by a thin polypyrrole (PPy) film covered with an assembly of magnetic nanoparticles (NPs). The magnetic particles were immobilized on PPy films under appropriate magnetic field in order to control their organization on the PPy film and finally to improve the sensitivity of the system in potential sensing applications. The electrical properties and morphology of the resulting PPy film and the PPy film/NPs composite were characterized with cyclic voltammetry, impedance spectroscopy (IS), scanning electron microscopy (SEM), atomic force microscopy (AFM) and infra-red spectroscopy (IR). By using streptavidin labeled magnetic particles it was possible to functionalize the NPs assembly with biotin-Fab fragment K47 antibody. The designed biosensor had been successfully applied in rapid, simple, and accurate measurements of atrazine concentrations, with a significantly low detection limit of 5 ng/ml.

Keywords: Polypyrrole; Magnetic beads; Impedance spectroscopy; Biosensor; Nanoparticles

1. Introduction

Polypyrrole (PPy) is a semiconducting polymer that has proven to be relatively highly conductive, easy to synthesize, and environmentally stable [1–3]. PPy can be prepared by plasma and vapor phase polymerization techniques. In applications like coating dielectric materials, the most suitable process is the in situ chemical polymerization, because it provides relatively high conductivity as well as suitable thickness and uniformity of the film [2]. Moreover, PPy have been paid more attention due to their potential application values in microelectronics, microsystems, optical sensors and photoelectronic chemistry [4–6]. Most of the optical, electrical and morphologic properties of the PPy depend on the synthesis procedure as well as on the dopant nature.

In many recent works, PPy films are found to be associated with metallic nanoparticles (NPs) [7]. The development of such nanocomposites is essentially motivated by their high analytical sensitivity in sensing applications [8]. Different properties emerging from the nanostructuration with NPs are at the origin of the increased sensing sensitivity. The NPs size and high surface area have first the ability to facilitate direct and fast electron transfer between the nanocomposite and the transducer. Second, when compared to homogeneous bulk matrices, the high surface area of the NPs assembly also leads to nanoporosity for signal amplifications and increased sensitivity toward surface adsorption or surface reactions [9–11]. Because of the same geometric properties the NPs assembly also allows minimum diffusion of the target molecule, and in the same time, miniaturization of the device. Finally it was shown that the selectivity of the sensor could be enhanced by tuning the molecular interactions between the NPs and linker molecules. The improvement of the sensing properties resulting from the nanostructuration is such that various routes were proposed in order to incorporate NPs either in the PPy film [12–16] or by synthesis of the metallic NPs directly on the PPy film [17–19].

In this work, PPy films were prepared by electropolymerization and covered in a second step by streptavidin labeled

* Corresponding author. Tel.: +33 3 89 60 87 18; fax: +33 3 89 60 87 99.
E-mail address: l.vonna@uha.fr (L. Vonna).

0039-9140/$ – see front matter © 2007 Elsevier B.V. All rights reserved.
doi:10.1016/j.talanta.2007.12.034

magnetic particles using a controlled magnetic field. This method allowed us to control the distribution and morphology of the NPs assembly on the PPy film for improved sensing applications. Electrical and morphological properties of both NPs covered and uncovered films, were assessed by using voltammetry, impedance spectroscopy (IS), scanning electron microscopy (SEM), atomic force microscopy (AFM) and infrared spectroscopy (IR). In order to test the performance of this nanocomposite electrode in biosensing applications, biotin-Fab fragment K47 was immobilized on the streptavidin labeled magnetic particles. This system was successfully used in detecting atrazine with a detection limit of 5 ng/ml.

2. Experimental

2.1. Chemicals and particles

Pyrrole monomer (98%) and lithium perchlorate ($LiClO_4$) was purchased from Sigma–Aldrich (France). Atrazine was purchased from Supelco, Bellefonte, Pennsylvania, USA. The antibody Fab 60 fragment K47 was obtained from Technische Universität München, Germany, and then labeled with biotin in the Institut National de la Recherche Agronomique (INRA), Paris, France. The buffer solution used for all experiments was phosphate buffered saline (PBS) containing 140 mM NaCl, 2.7 mM KCl, 0.1 mM Na_2HPO_4, 1.8 mM KH_2PO_4, pH 7 and the redox couple $Fe(CN)_6^{3-}/Fe(CN)_6^{4-}$ at a 5 mM concentration. All reagents were of analytical grade and ultrapure water (resistance 18.2 MΩ cm^{-1}) produced by a MilliporeMilli-Q system was used. The magnetic particles coated with streptavidin are Fe_2O_3 particles characterized by a mean diameter of 200 nm and purchased from Ademtech SA, Pessac, France.

2.2. Gold electrodes cleaning

The gold electrodes were cleaned with organic solvents (acetone and ethanol) and with piranha solution (1:3 H_2O_2—concentrated H_2SO_4) for 1 min. After each treatment, the gold substrates were rinsed with ethanol and dried under nitrogen flow.

2.3. Electropolymerization

The PPy film was coated on a gold electrode using cyclic voltammetry. The gold electrode was bulked in an acetonitril solution (Bu_4NPF) containing pyrrole monomer (C_4H_5N 0.1 M) and lithium perchlorate ($LiClO_4$ 0.1 M). The potential sweep was used instead of a polymerization in potentiostatic mode in order to obtain a smoother film. The potential sweep was performed from −300 to 1100 mV with 25 mV/s scan rate for 6 cycles. Three-electrodes cells were used, a platinum as counter electrode, calomel reference electrode and gold substrate as working electrode.

2.4. Cyclic voltammetry

Cyclic voltammetry measurement was performed in a 5 mM solution of redox couple $Fe(CN)_6^{-4/-3}$ prepared in PBS buffer. Scanning potential was conducted between −600 and 600 mV with 100 mV/s scan rate. Cyclic voltammetry enabled the detection of PPy and magnetic beads film immobilized on gold surface.

2.5. Impedance spectroscopy

The impedance analysis was performed with the Volta-lab 40 impedance analyser in the frequency range 0.05 Hz to 100 kHz, using a modulation voltage of 10 mV. A three-electrode system was employed with a saturated calomel electrode (SCE), an immunosensor working electrode (0.11 cm^2), and a platinum strip counter electrode (0.54 cm^2). The impedance measurements were performed in the presence of a 5 mM $K_3[Fe(CN)_6]/K_4[Fe(CN)_6]$ (1:1) mixture as redox probe in PBS.

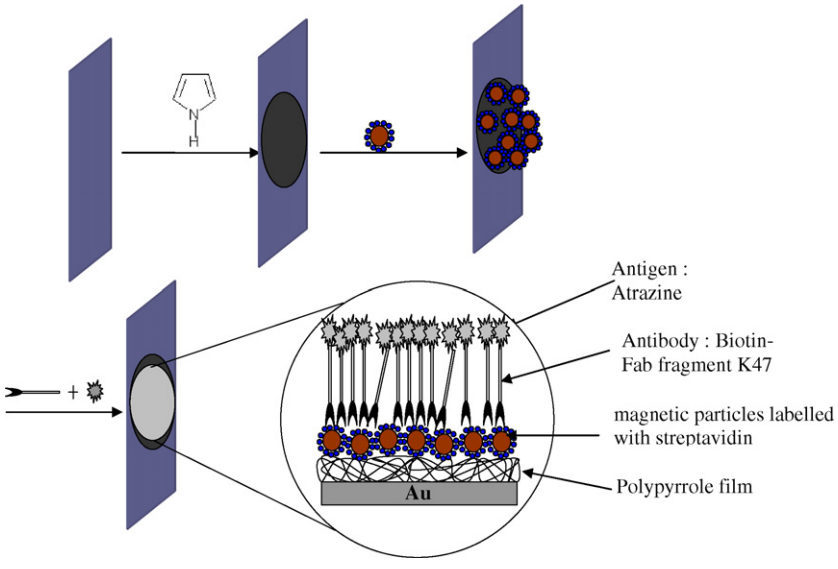

Fig. 1. A schematic diagram of the immunosensor showing the stepwise immunosensor fabrication process.

The measured spectra of the impedance was analysed in terms of electrical equivalent circuits model using a Zview modelling programme (Scribrer and associates, Charlottesville, VA). All electrochemical measurements were carried out at room temperature and in a faraday cage. More details on electrochemical impedance spectroscopy (EIS) can be found in Refs. [20–23].

2.6. Scanning electron microscopy

Electron micrographs of gold electrode functionalized with PPy, with and without the NPs assembly, were observed with a FEI QUANTA 400 model scanning electron microscope (SEM) working at an accelerating voltage of 30 keV. Since this electrode is a conducting material all observations were preformed without any prior gold sputtering.

2.7. Atomic force microscopy

Electrode surfaces were imaged with a D3000 AFM from Digital Instruments. All images were acquired in the tapping mode, processed by means of a plane fit and finally flattened in the first mode using a built-in software procedure. Because of the high roughness of the PPy electrode surface, the scan rate we applied was relatively low (0.1–0.5 Hz).

2.8. Fourier transformed infra-red spectroscopy

Burcker IFS66VIS spectrometer equipped with a middle infrared (MIR) source, a DTGS detector and a KBr separating mirror was used to obtain the FTIR spectra. Our method consisted on recording the spectrum of the cleaned gold substrate and then the gold substrate with PPy film. The spectrum of the cleaned electrode served as a reference. The ratio of the two spectra gave the spectrum of the PPy. The same method was used to confirm the deposition of the functionalized streptavidin labeled magnetic NPs.

3. Results and discussion

3.1. Cyclic voltammetry

Cyclic voltammetry is an electrochemical technique, which can be used to study the kinetics of oxido-reduction reaction on material, their insulating and conducting properties. The molecular structure of the biosensor developed in this work is shown in Fig. 1. Cyclic voltammograms of the gold electrode (Fig. 2a) shows a reversible phenomenon, which is the typical behaviour of gold surface with redox couple. The two peaks of the cathodic and anodic waves of redox probe have been obtained. After modification of the gold surface with PPy, the dc-current increases due to the conducting properties of the PPy film (Fig. 2b). After immobilization of the magnetic particles on the PPy film, the direct current decreases due to the insulating properties of the functionalized film (streptavidin) covering the particles (Fig. 2c). The same explanation applies for the decrease of the direct current after immobilization of the antibody (Fig. 2d) and after the BSA blocking step (Fig. 2e). To confirm all these results, impedance spectroscopy measurements were performed on those systems.

3.2. Impedance spectroscopy

EIS has been widely recognized as a powerful diagnostic tool for the investigation of the electrical behaviour of an electrochemical system in which various processes proceed at different rates [23–27,20]. The EIS can further give information on the impedance changes of the immunoelectrode surface

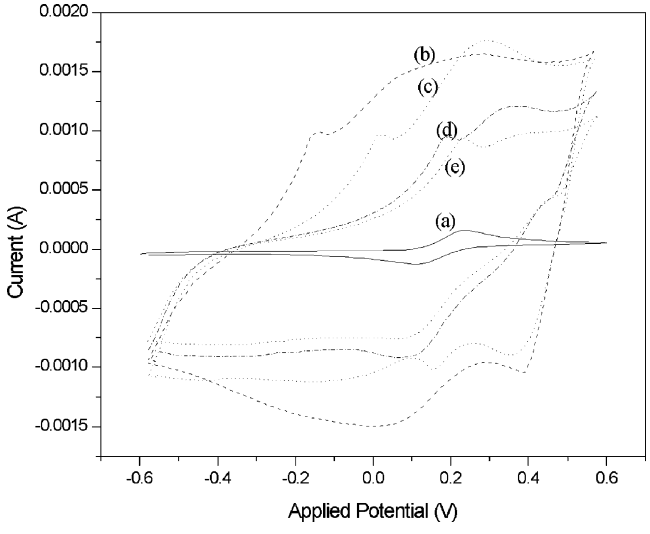

Fig. 2. Cyclic voltammograms (CVs) with 100 mV s^{-1} scan rate in a 5 mM $Fe(CN)^{-4/-3}$ solution (PBS, pH 7.0), after different steps of modification: (a) bare gold electrode, (b) PPy film modified gold electrode, (c) PPy covered with streptavidin labeled magnetic particles, (d) immobilization of the antibody biotin-Fab fragment K47 and (e) BSA blocking layer.

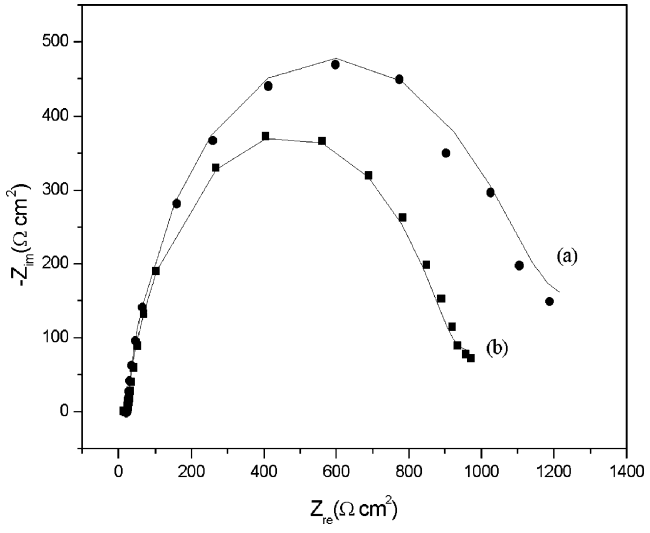

Fig. 3. Nyquist diagram (Z_{re} vs. Z_{im}) for the faradic impedance measurements corresponding to (a) bare Au-electrode and (b) PPy film functionalized Au-electrode. All measurements were performed in PBS (pH 7.0) + 5 mM $Fe(CN)_6^{-4/-3}$ solution. Amplitude of alternating voltage 10 mV. Solid curves show the computer fitting of the data using the equivalent circuits shown in Fig. 4.

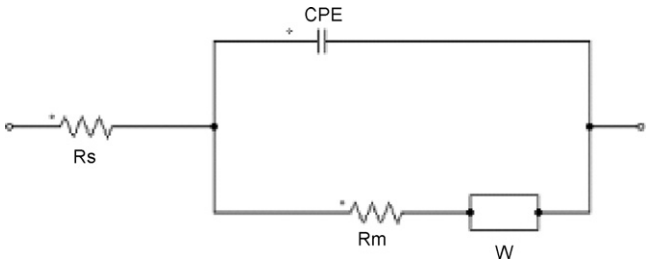

Fig. 4. Equivalent circuit used for impedance spectra.

in the modification process. The complex impedance can be presented as a combination of the real impedance (Z_{re}) and imaginary impedance (Z_{im}), Nyquist plot. Typical Nyquist plots for gold electrode and gold/PPy film from 50 mHz to 100 kHz at −1200 mV potential (versus calomel electrode), with 5 mM redox couple, are shown in Fig. 3. A more stable PPy film in liquid medium was obtained for an applied electrical potential of −1200 mV versus calomel electrode. Impedance spectra may be interpreted through equivalent circuits representing the different processes involved in the description of the system with discrete electric elements. We have used in the present work the Randles equivalent circuit modified by inclusion of distributed elements to take into account the finite spatial extension of the system under study [25,26,20]. This latter manifest in impedance spectra as 'depressed' semicircles, with their origin located below the real axis. The equivalent circuit used for the interpretation of the data is shown in Fig. 4, diffusion is represented by Warburg element. A CPE was thus used to represent the non-homogeneous nature of the electrode material, the electrode material and the distribution of relaxation time of the processes occurring within it, with impedance given by [25,26,20]:

$$Z = \left(\frac{1}{\sigma}\right)(j\omega)^{-\alpha}$$

where σ and α are positive constants.

A CPE describes a capacitor when $\alpha = 1$, in which case $\sigma = C$, and tends to a resistor as $\alpha \to 0$. The presence of a CPE with $0 < \alpha < 1$ depresses high frequency semicircles below the real axis. The semicircle diameter of EIS equals the electron transfer resistance, R_m. This resistance controls the electron transfer kinetics of the redox probe at the electrode interface. Curve a in Fig. 3 shows EIS of the bare gold electrode.

It can be seen that the bare gold electrode exhibits a semicircle giving the resistance equal to 1020 Ω cm^2. After the bare gold electrode was modified with PPy film, the EIS of the modified electrode shows a lower interfacial resistance equal at 849.7 Ω cm^2 (curve b in Fig. 3). The decrease in R_m resistance indicates an increase in the conductivity, which confirms the results obtained with cyclic voltammetry.

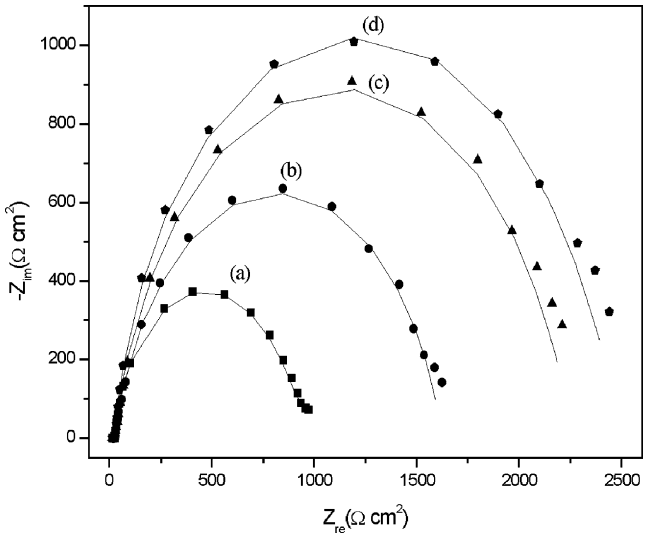

Fig. 5. Nyquist diagram for the faradic impedance measurements corresponding to (a) PPy film/Au-electrode, (b) streptavidin labeled magnetic particles/PPy film/Au-electrode, (c) biotin-Fab fragment K47 antibody/streptavidin labeled magnetic particles/PPy film/Au-electrode and (d) blocked layer with BSA/biotin-Fab fragment K47 antibody/streptavidin labeled magnetic particles/PPy film/Au-electrode. Solid curves show the computer fitting of the data using the equivalent circuits shown in Fig. 4. Symbols show the experimental data.

The PPy film was covered with magnetic particles labeled with streptavidin using a magnetic field (0.3 mT). Fig. 5 shows the impedance spectrum of a PPy film coated gold electrode (curve a) compared with streptavidin labeled magnetic particles surface (curve b), with an antibody-immobilized surface (curve c) and with BSA blocking layer (curve d). Note that all the spectra are almost similar, containing a distorted semicircle. The diameter of the semicircle provides an estimate of the film charge transfer resistance. Using the same equivalent circuit model described in Fig. 4, an excellent fitting between the simulation and experimental spectra was obtained. The values obtained for the different elements composed the equivalent circuit are shown in Table 1. The resistance of the studied interface increases after the immobilization of each step. This increase is due to the decrease of the conductivity due to the insulating properties of grafted layers. This confirms the results obtained with cyclic voltammetry.

Table 1
Fitting values of the equivalent circuit elements for PPy, magnetic layer, after binding of the antibody and blocking with BSA

	PPy film	Streptavidin labeled magnetic particles	Antibody: biotin-Fab fragment K47	Blocking layer: BSA
R_s(Ω cm^2)	24.26	24.23	22.95	24.36
R_m (Ω cm^2)	849.7	1593	2196	2377
σ (μF cm^{-2})	71.77	86.77	85.52	82.08
α	0.9	0.84	0.86	0.9
W (mΩ cm^2)	12.67	60	50	23

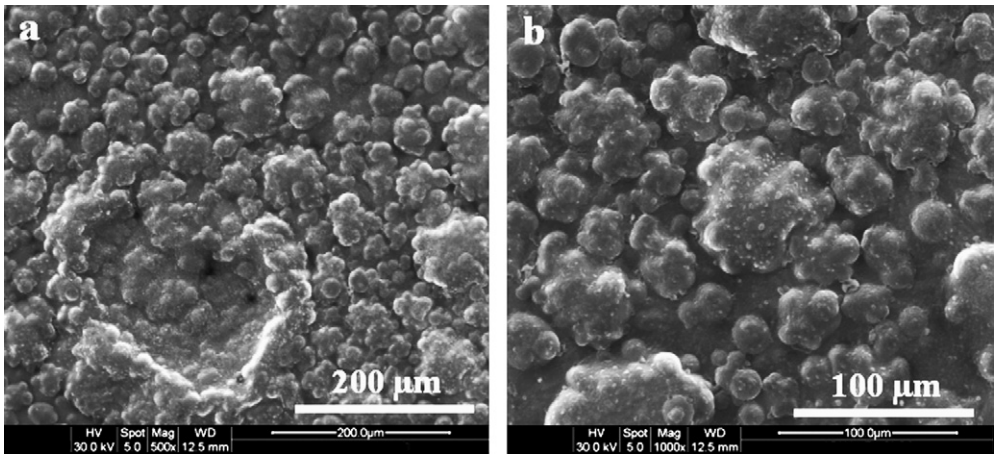

Fig. 6. SEM micrographs of the PPy film formed on gold electrode.

3.3. Scanning electron microscopy

Fig. 6 shows two SEM micrographs of a PPy film surface formed after 6 deposition cycles. These micrographs reveal the cauliflower morphology usually observed for electrochemically deposited PPy films which is attributed to the nodular fractal-type growth of these polymers [28,29]. SEM observations associated with optical microscopy observations showed that such a film grew uniformly over the whole surface of the electrode. After deposition of the NPs, the surface of the PPy film seems to be smoother and the cauliflower structure is less pronounced as shown in Fig. 7a and b. Moreover cracks are clearly observable in the NPs assembly probably due to constraints emerging during the drying step. The side view of the PPy film/NPs assembly composite shown in Fig. 7c and d were observed after breaking the sample in two parts. One can clearly see the thicknesses of both the PPy film and the NPs assembly which are, respectively around 2 and 4 μm. The morphology of the NPs assembly shown in this image fulfill the porosity and large surface area conditions for high sensitivity of the sensor. Wrinkling of the PPy film may come from the fracture of the sample.

3.4. Atomic force microscopy

The atomic force microscopy images of the PPy film shown in Fig. 8 confirm the SEM observations at the microscopic scale. The micrometric structure of the polymer is still characterized by a cauliflower morphology as expected for a fractal morphology [30]. However, the high roughness of this surface does not allow

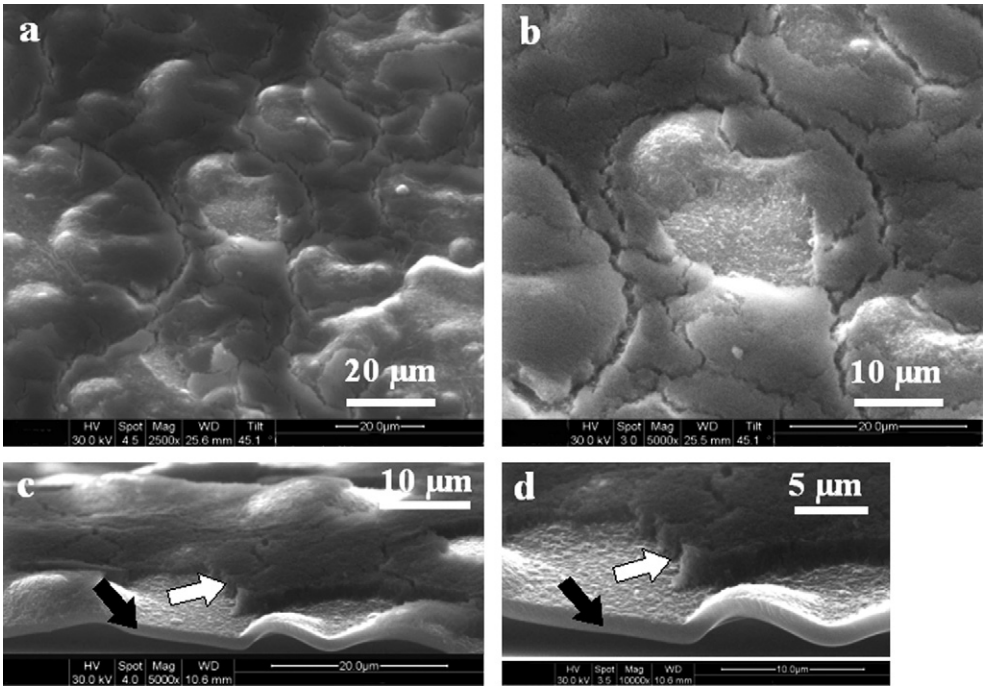

Fig. 7. SEM micrographs of the magnetic NPs assembly covering the PPy film. Top view (a) and (b), side view (c) and (d). The black arrow indicates the PPy film and the white arrow the NPs assembly.

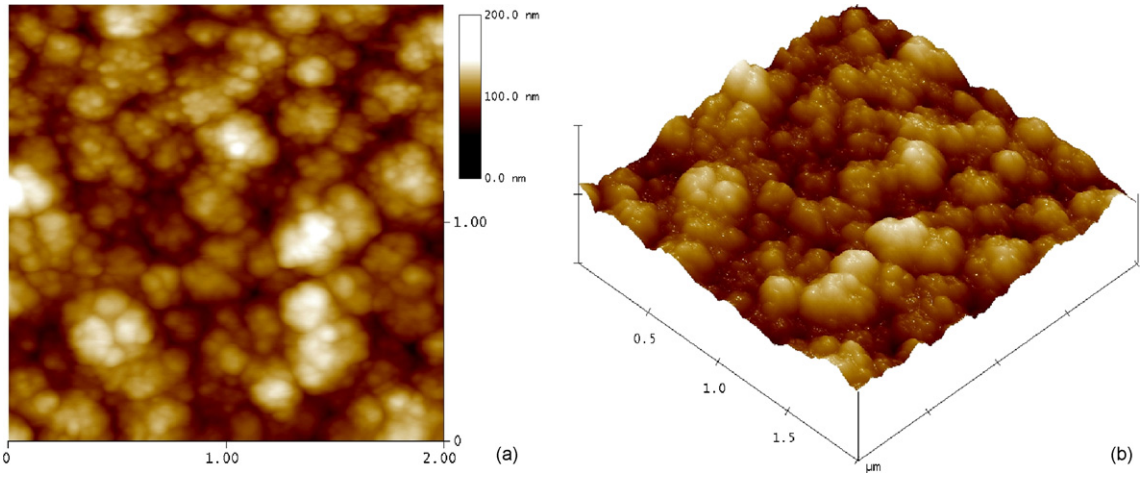

Fig. 8. Top (a) and 3D (b) AFM images of a PPy film showing the cauliflower structure of this polymer. *Z* range on the 3D view is 200 nm.

atomic force microscopy acquisitions on large area. The NPs assembly is clearly observable with atomic force microscopy as shown in Fig. 9. Cracks in the NPs assembly are again present at microscopic scale as under SEM at larger scale. Both SEM and AFM observations allow us to assess for the distribution of both the PPy and the NPs on the electrode, which should provide enhanced adsorption and sensitivity in sensing application.

3.5. FTIR

The infrared absorption spectra of PPy films without and with functionalized magnetic particles are shown in Fig. 10. The shown spectra is nearly same in the two cases, indicating that the structure of PPy film was not changed after particles immobilization. The broad band at 3440 cm^{-1} corresponds to the absorption of N–H stretching vibration mode. The absorption at 1635 and 1554 cm^{-1} assigned to the C=C and C–C ring stretching mode, respectively. The bands at 1365 and 1189 cm^{-1} are assigned to C–H and C–N stretching vibrations [31–34]. The peaks located at 907, 786 and 676 cm^{-1} should be assigned to C–H out-of-plane deformation, C–H out-of-plane ring deformation and C–C out-of-plane ring deformation, respectively [35,36]. No peak has been observed at 1700 for C=O stretching, which suggests that the pyrrole is not overoxidized. After the immobilization of streptavidin functionalized magnetic particles, the measured spectra shows an increase of the peak intensity below 1500 cm^{-1} and the presence of a band located at 2040 cm^{-1}. This band is attributed to one of the vibrations mode of streptavidin.

3.6. Biosensor application

Atrazine (2-chloro-4-ethytlamino-6-isopropylamine-1,3,5-triazine) is a worldwide and commonly used herbicide. Despite it is usually considered toxic only at high doses, it was shown recently that atrazine may interfere with metamorphosis and sex differentiation even at low and ecologically relevant doses [37]. The detection of this pollutant is of fundamental importance for environmental safety and human health. In this work biotinylated Fab fragment K47 was covalently bound to the particles through streptavidin/biotin linkage. This allows specific bounding of atrazine on the NPs and variation of the electrode impedance response. Atrazine–antibody interactions were mon-

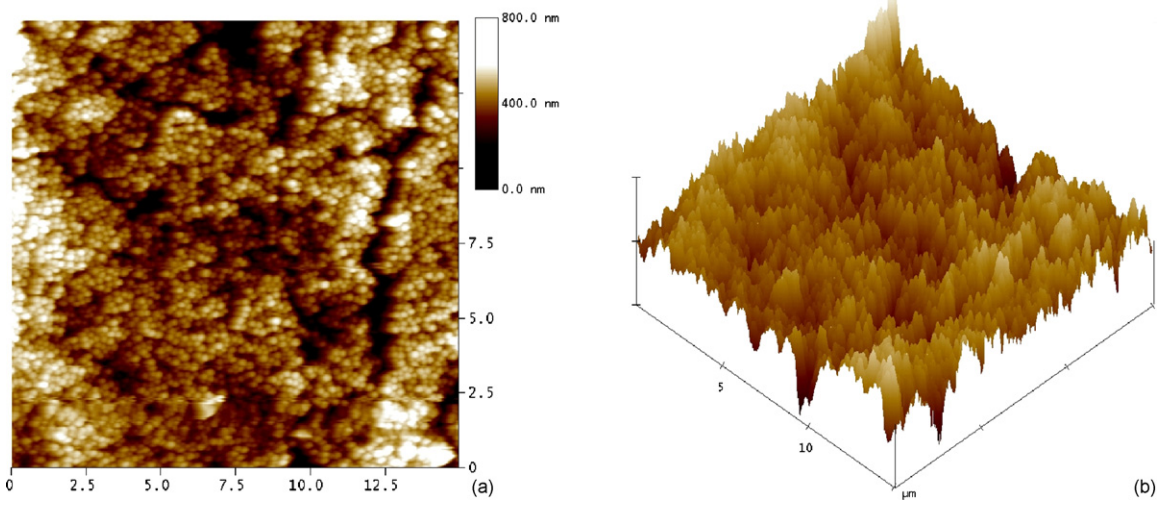

Fig. 9. Top (a) and 3D (b) AFM images of a PPy film (6 cycles) covered with an array of nanoparticles. *Z* range on the 3D view is 600 nm.

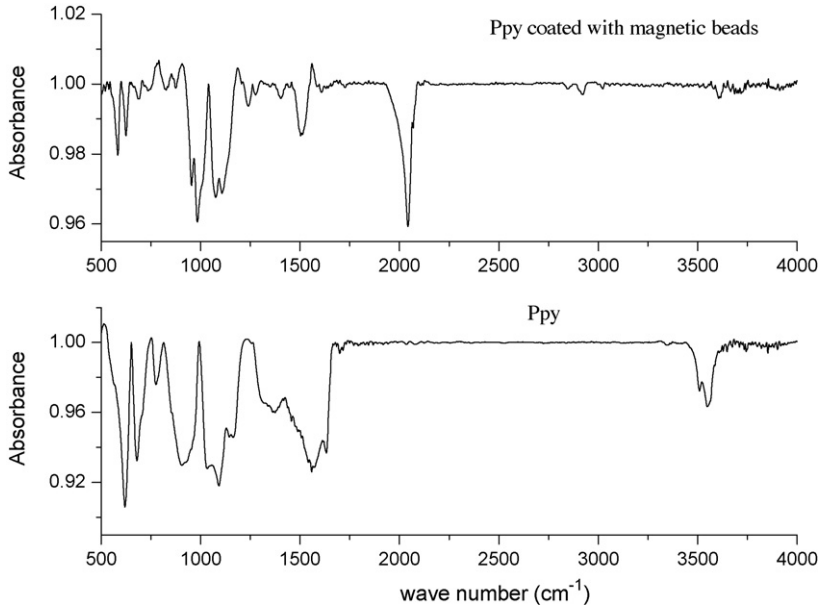

Fig. 10. FTIR spectra for pure PPy film and PPy/streptavidin labeled magnetic particles.

itored by impedance spectroscopy at −1200 mV. The impedance variation after atrazine injections in the range of 0–70 ng/ml are shown in Fig. 11. The semicircle diameter in the Nyquist plot is increasing with the atrazine concentration, implying that more amount of atrazine was linked to the interface.

The change of the charge transfer resistance ΔR is obtained by subtracting the resistance of the immobilized BSA layer from the resistance of the resultant immuno-complex. As for the control, ΔR is obtained by deducting the resistance of the PPy/BSA film from the resistance of the antibody–atrazine complex. Fig. 12 shows an increase in the charge transfer resistance ΔR with the increment of atrazine concentration in the range of 0–170 ng/ml. These results revealed that the presence of the

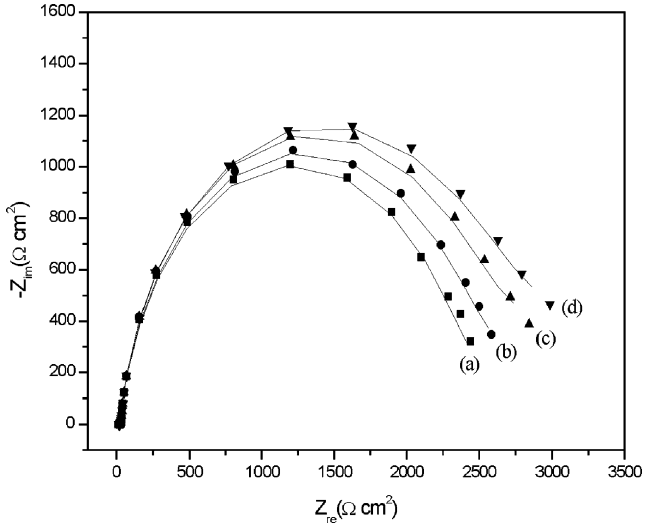

Fig. 11. Complex impedance plots of antigen–antibody/streptavidin labeled magnetic particles/PPy film/Au-electrode under various concentrations of antigen. The concentrations of antigen (ng/ml): (a) 0; (b) 5; (c) 10; (d) 70. Applied frequency from 0.5 Hz to 100 kHz.

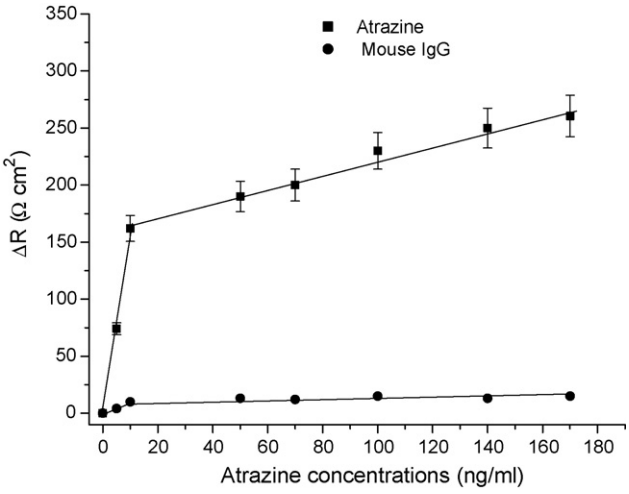

Fig. 12. Calibration plots for the immunosensor in PBS + 5 mM $Fe(CN)_6^{-4/-3}$ solution at pH 7.0 in the presence of different concentrations of atrazine and non-specific antigen.

PPy film under the NPs assembly increases over four orders of magnitude the sensitivity of the sensor as compared to only the NPs assembly, with an excellent detection limit of 5 ng/ml [38]. Whereas the response of the immunosensor to different concentrations of non-specific molecules (IgG mouse antigen) was clearly non-significant.

4. Conclusion

In this work, we report the preparation and characterization of a nanocomposite PPy/NPs films for biosensor applications. An assembly of magnetic particles labeled with streptavidin was immobilized on the PPy film under appropriate magnetic field. In a second step, biotin-Fab fragment K47 antibody was coupled to the particles through streptavidin for atrazine detection.

The designed biosensor is characterized by high sensitivities and low detection limits (5 ng/ml atrazine or 2.3×10^{-8} M). This study demonstrates that the assembling of magnetic NPs under magnetic field on conductive polymer films (PPy for example), is a convenient way to construct easily and rapidly sensitive nanocomposites electrodes. The NPs assembly on the PPy film was shown to be uniform and stable enough to be used in biosensing applications, and suggests that the method developed in this work could be useful for the fabrication of other biological sensors.

Acknowledgments

The authors thank the Alexander Von Humboldt Foundation for material donation, Pr. N. Jaffrezic–Renault (UCB, Lyon1, France) and Hamidou Haidara (Institut de Chimie des Surfaces et Interfaces—CNRS, UPR9069, Mulhouse, France) for scientific support.

References

[1] L.-X. Wang, X.-G. Li, Y.-L. Yang, React. Funct. Polym. 47 (2001) 125.
[2] M. Ferenets, A. Harlin, Thin Solid Films 515 (2007) 5324.
[3] M.A. de la Plaza, M.C. Izquierdo, Eur. Polym. J. 42 (2006) 1446.
[4] W. Geng, N. Li, X. Li, R. Wang, J. Tu, T. Zhang, Sens. Actuator B 125 (2007) 114.
[5] M. Liu, Y. Zhang, M. Wang, C. Deng, Polymer 47 (2006) 3372.
[6] A. Hallik, A. Alumaa, J. Tamm, V. Sammelselg, M. Väärtnõu, A. Jänes, E. Lust, Synth. Met. 156 (2006) 488.
[7] R. Gangopadhyay, A. De, Chem. Mater. 12 (2000) 608.
[8] C.W. Welch, R.G. Compton, Anal. Bioanal. Chem. 384 (2006) 601.
[9] K.R. Brown, A.P. Fox, M.J. Natan, J. Am. Chem. Soc. 118 (1996) 1154.
[10] T.G. Drummond, M.G. Hill, J.K. Barton, Nat. Biotechnol. 21 (2003) 1192.
[11] A.N. Shipway, M. Lahav, L. Willner, Adv. Mater. 12 (2000) 993.
[12] J.L. Besombes, S. Cosnier, P. Labbe, Talanta 44 (1997) 2209.
[13] A.C. Arango, S.A. Carter, P.J. Brock, Appl. Phys. Lett. 74 (1999) 1698.
[14] P. Zhang, Z.H. Yang, D.J. Wang, S.H. Kan, X.D. Chai, J.Z. Liu, T.J. Li, Synth. Met. 84 (1997) 165.
[15] Y.C. Liu, H.T. Lee, S.J. Yang, Electrochim. Acta 51 (2006) 3441.
[16] A. Alqudami, S. Annapoorni, P. Sen, R.S. Rawat, Synth. Met. 157 (2007) 53.
[17] X.J. Zhou, A.J. Harmer, N.F. Heinig, K.T. Leung, Langmuir 20 (2004) 5109.
[18] Y. Li, G.Q. Shi, J. Phys. Chem. B 109 (2005) 23787.
[19] J. Li, X. Lin, Sens. Actuator B 124 (2007) 486.
[20] A. Abdelghani, S. Hleli, K. Cherif, Mater. Lett. 56 (2002) 1064.
[21] Y. Hou, S. Helali, A. Zhang, N. Jaffrezic-Renault, C. Martelet, J. Minic, T. Gorojankina, M.-A. Persuy, E. Pajot-Augy, R. Salesse, F. Bessueille, J. Samitier, A. Errachid, V. Akimov, L. Reggiani, C. Pennetta, E. Alfinito, Biosens. Bioelectron. 21 (2006) 1393.
[22] S. Hleli, A. Abdelghani, A. Tlili, Sensors 3 (2003) 472.
[23] S. Hleli, C. Martelet, A. Abdelghani, N. Burais, N. Jaffrezic-Renault, Sens. Actuator B 113 (2006) 711.
[24] J.R. MacDonald, Impedance Spectroscopy, Wiley, New York, 1987.
[25] H. Hillebrandt, A. Abdelghani, C. Abdelghani, E. Sackmann, Appl. Phys. A 73 (2001) 539.
[26] Wiegand, PhD thesis: Fundamental principles of the electric properties of supported lipid membranes investigated by advanced methods of impedance spectroscopy, 1999, Shaker verlag, Technishe Universität of München, Germany, ISBN 3-8265-7231-9.
[27] A. Tlili, A. Abdelghani, S. Hleli, M.A. Maaref, Sensors 4 (2004) 105.
[28] S. Paschen, M. Carrard, B. Senior, F. Chao, M. Costa, L. Zuppiroli, Acta Polym. 47 (1996) 511.
[29] R. Singh, A.K. Narula, R.P. Tandon, S.U.M. Rao, V.S. Panwar, A. Mansingh, S. Chandra, Synth. Met. 79 (1996) 1.
[30] T. Silk, Q. Hong, J. Tamm, R.G. Compton, Synth. Met. 93 (1998)59.
[31] J. Zhu, J.Z. Xu, J.T. He, Y.J. Wang, Q. Miao, H.Y. Chen, Anal. Lett. 36 (2003) 1547.
[32] Y.Q. Miao, J.G. Guan, Anal. Lett. 37 (2004) 1053.
[33] J. Li, H. Zhan, Y. Zhou, Electrochem. Commun. 5 (2003) 555.
[34] M. Bazzaoui, E.A. Bazzaoui, L. Martins, J.I. Martins, Synth. Met. 130 (2002) 73.
[35] P. Dutta, S.K. De, Synth. Met. 139 (2003) 201.
[36] M. Omastová, M. Trchová, J. Pionteck, J. Prokeš, J. Stejskal, Synth. Met. 143 (2004) 153.
[37] T.B. Hayes, A. Collins, M. Lee, M. Mendoza, N. Noriega, A.A. Stuart, A. Vonk, Proceedings of the National Academy of Sciences of the United States of America 99, 2002, p. 5476.
[38] S. Helali, C. Martelet, A. Abdelghani, N. Jaffrezic-Renault, Electrochim. Acta 51 (2006) 5182.